The Search of Diffusive Properties in Ambient Seismic Noise

By

José Piña-Flores [1-2], Martín Cárdenas-Soto [2],

Antonio García-Jerez [3], Michel Campillo [4] and Francisco J Sánchez-Sesma [5]

(1) Facultad de Ingeniería, Universidad Nacional Autónoma de México; CU, Circuito Escolar; Coyoacán 04510 CDMX, Mexico. Email: jpf@unam.mx and martinc@unam.mx
(2) Posgrado de Ingeniería, Universidad Nacional Autónoma de México; Edificio "S" "Bernardo Quintana Arrioja", Primer Piso, Facultad de Ingeniería, CU, Coyoacán 04510 CDMX, Mexico.
(3) Grupo de Investigación en Geofísica Aplicada, Universidad de Almería; La Cañada de San Urbano, s/n, 04120 Almería, Spain. Email: agj574@ual.es
(4) Institut des Sciences de la Terre, Universite Grenoble Alpes, Grenoble, F-38401, France. E-mail: michel.campillo@univ-grenoble-alpes.fr
(5) Instituto de Ingeniería, Universidad Nacional Autónoma de México, CU, Coyoacán 04510 CDMX, Mexico. E-mail: sesma@unam.mx

Accepted date: 26 January 2021. Received date: 25 May 2020.

Corresponding author: José Piña-Flores. jpf@unam.mx

Key Points:

- We explore the stabilization of P-wave and S-wave energy in pre-event and post-event earthquake records.

- We show clear evidence that seismic energy equipartition is present in the ambient seismic noise records.

- The stabilization of the P- to S-wave energy ratio is a process which anticipates the diffusion regime.

Keywords:

Ambient seismic noise, Energy equipartition, Earthquake

Abstract

Ambient seismic noise (ASN) is becoming of interest for geophysical exploration and engineering seismology as it is possible to exploit its potential for imaging. Theory asserts that the Green's function can be retrieved from correlations within a diffuse field. Surface waves are the most conspicuous part of Green's function in layered media. Thus, the velocities of surface waves can be obtained from ASN if the wavefield is diffuse. There is widespread interest in the conditions of emergence and properties of diffuse fields. In the applications, useful approximations of the Green's function can be obtained from cross-correlations of recorded motions of ASN. An elastic field is diffuse if the illumination is azimuthally uniform and equipartitioned. It happens with the coda waves in earthquakes and has been verified in carefully planned experiments. For one of these data sets, the 1999 Chilpancingo (Mexico) experiment, there are some records of earthquake pre-events that undoubtedly are composed of ASN, so that the processing for coda can be tested on them. We decompose the ASN energies and study their equilibration. The scheme is inspired by the original experiment and uses the ASN recorded in an L-shaped array that allows the computation of spatial derivatives. It requires care in establishing the appropriate ranges for measuring parameters. In this search for robust indicators of diffusivity, we are led to establish that under certain circumstances, the S and P energy equilibration is a process that anticipates the diffusion regime (no necessarily isotropy), which justifies the use of horizontal-to-vertical spectral ratio in the theoretical context of diffusion.

Introduction

In recent years, Ambient Seismic Noise (ASN) has been widely used in geophysical exploration and engineering seismology. This ubiquitous excitation is a combination of oceanic, atmospheric, seismic and human contributions (see *e.g.,* Asten and Henstridge, 1984; Ardhuin *et al*., 2011). Although the sources of noise associated with different frequency bands are not known precisely, it has been found that for low frequency ($f < 0.3\ Hz$) the ASN may be dominated by interactions of the ocean with the solid Earth (Friederich *et al*., 1998; Rhie and Romanowicz, 2004; Ardhuin *et al*., 2011). On the other hand, the ASN is produced locally by human activity and wind at a higher frequency($f > 0.3\ Hz$). Due to the attenuation in subsoil materials, this high-frequency noise cannot be propagated at great distances. The ASN comes mainly from shallow sources that mostly generate surface waves (Campillo, 2006).

The first systematic works with ASN at the beginning of the last century are due to Kanai (see Kanai *et al.*, 1954). Later, in a pioneering work, Aki (1957) studied the spatial autocorrelation (SPAC method) of ASN. In this technique, the azimuthal average of the correlation coefficient of the vertical motion of ASN allows evaluating the phase velocity of Rayleigh surface waves. The treatment of horizontal components allows the retrieval of Love wave velocities. Note that this approach takes advantage of the natural illumination of seismic noise. Also, it has been shown that it is possible to obtain the most conspicuous part of the Green function in a layered system by cross-correlation of ASN between two receivers. Shapiro and Campillo (2004), Sabra *et al.* (2005), and Shapiro *et al*. (2005) used long-range cross-correlations for practical applications in seismology.

Since then, numerous studies worldwide have used this technique to retrieve empirical Green functions and extract the dispersion curves of Rayleigh and Love surface waves, which are propagation velocities as functions of frequency. For example, there are tomography maps of phase and group velocities for different parts of the world. These maps correlate well with the geology and tectonics of the region and, in some cases, they revealed new features. Let us mention the work by Shapiro and Campillo (2004); Shapiro *et al.* (2005) and Ritzwoller *et al.* (2011) for North America, the research by Ward *et al.* (2013) in South America, of Yang *et al*. (2007) for Europe and Gudmundsson et al. (2007) for Iceland, and the study by Zheng *et al.* (2008) for Asia. Saygin and Kennett (2010) considered New Zealand and Australia, and Gudmundsson *et al.* (2007) dealt with New Zealand and Australia.

Likewise, since Sánchez-Sesma *et al.* (2011a) established the relationship between the horizontal-to-vertical spectral ratio (HVSR), proposed by Nakamura (1989, 2000), with the imaginary parts of the Green function, several studies (Spica *et al.,* 2015; García-Jerez *et al.,* 2016 and Piña-Flores *et al.,* 2017, García-Jerez *et al.,* 2019) have been carried out in order to obtain velocity profiles as a function of depth through inversion. Also, Matsushima *et al.* (2017), Perton *et al.* (2018) and Piña-Flores *et al.,* (2021) considered the lateral irregularity. The success of these studies can be explained because they relate the observed HVSR with its model counterpart in terms of the Green functions which are intrinsic properties of layered systems. This relationship implies the assumption that the ASN is a diffuse field, and therefore, it can be regarded as the by-product of isotropic illumination of random waves. From this perspective, the ambient noise sources are random and the generated seismic waves in their propagation suffer multiple diffractions due to the medium heterogeneities (Campillo, 2006). According to Shapiro *et al.* (2000) a diffusive regime is reached when the distribution of seismic energy (sources and secondary sources) is almost isotropic and the phase is random as a result of multiple scattering. If the medium does not have significant lateral irregularity the ideal illumination conditions can be checked in reality. In the presence of irregularities, the field isotropy cannot be verified but the field could still be diffusive. In Sánchez-Sesma *et al.* (2006) and Pérez-Ruiz *et al.* (2008), one sees that uniform illumination in the system's envelope produces a diffuse field that near the scatters it is not isotropic.

According to Weaver (1982; 1985), two simple definitions of a diffusive regime can be conceived. The first considers a diffuse field at a given frequency as a state of vibration for which the normal modes of the system are in statistical equilibrium. In this definition, seismic energy is distributed among all normal modes according to the Principle of Equipartition. This principle states that all modes (which together constitute a diffuse field), appropriately normalized, contribute the same energy to construct the Green function if they are summed up. Some relevant connections between analytic and deterministic solutions arise from diffuse field theory (see Sánchez-Sesma *et al.,* 2011b, Pérez-Ruiz *et al.,* 2008; Perton and Sánchez-Sesma, 2016). The second and most popular definition asserts that for each point of the medium in vibration, the diffuse field can be represented as an isotropic and random superposition of plane waves. Each one has amplitude that varies slowly over time and with a random phase (Shapiro *et al.,* 2000). This view implicitly assumes isotropy and neglects irregularity but can be regarded as the concept that applies to the illumination itself.

The first observation of energy equipartition in seismic records was the result of a carefully planned experiment in which the codas of 13 earthquakes recorded in a very small square array (c. 50m) in Guerrero (Mexico) were analyzed (Shapiro *et al*., 2000; Hennino *et al*., 2001). The seismic energies could be separated in terms of the squared curl modulus and the divergence of the field obtained numerically from spatial derivatives. The energy ratio could be computed, and they suggest that the stability of this ratio is a strong indicator that the wave field has a diffusive regime, in this case, for the seismic coda. They pointed out multiple diffraction in the coda of seismograms recorded in Guerrero, Mexico and, following Aki and Chouet (1975), excluded single scattering as an alternative explanation of the coda. In other experiment Margerin *et al.* (2009) study the potential and kinetic energies of the shear waves in the ten-earthquake codas recorded at Pinyon Flats Observatory, California. They demonstrated a clear stabilization of the relationship between P wave and S wave (W_S/W_P) energies in the coda, with similar values for the ten earthquakes studied, interpreting these observations as an energy equipartition signature. On the other hand, full wavefield simulations both in acoustics and dynamic elasticity (Papanicolaou *et al.,* 1996; Przybilla *et al.,* 2006) demonstrated that in a diffusive regime, the ratio of the energy densities of the P and S waves stabilizes to a constant.

In the literature, various works found that ambient field is not fully diffuse (Weaver *et al.*, 2009; Mulargia (2012), Sens-Schonfelder *et al.,* 2015; Liu and Ben-Zion, 2016). For example, Mulargia (2012) developed a procedure to establish the applicability of the diffuse field paradigm to ambient seismic noise. His method is based on azimuthal isotropy and spatial homogeneity and was applied to ASN recorded in 65 sites covering a wide variety of environmental and subsurface conditions. Mulargia (2012) asserts that seismic noise is not diffuse and that basic physical arguments suggest that diffuse-field theory may not be applicable to seismic noise, and notes that such a conclusion has no practical inhibitory effect on passive imaging. We think he overlooked multiple scattering roles and the field stabilization towards a state, non-necessarily an isotropic one.

In this work, we explore the stabilization of the W_S/W_P energy ratio in ASN records, and ASN windows in the preevent and postevent of some earthquakes, at different locations in Mexico. We use small arrays following the approaches of Shapiro *et al.* (2000), Hennino *et al*. (2001) and Margerin *et al*. (2009). Three sites were studied:

1. UNAM's main campus, South of Mexico City. Ambient seismic noise, ASN, was recorded at two nearby sites (the School of Engineering and the Sport Field) using L-shaped arrays of three sensors each recording for two hours.

2. La Primavera park in Zapopan, Jalisco, Mexico. ASN in post-event seismic data was recorded during three hours in a L-shaped array of three sensors. The M_w 7.1 earthquake of September 19, 2017 (SSN, 2020) was recorded as well.
3. Chilpancingo, Guerrero, Mexico. ASN in pre-event seismic data from a well-known experiment regarding the coda of 11 events in 1999 (see Shapiro *et al.*, 2000 and Hennino *et al.*, 2001) was re-analyzed for one of the earthquakes recorded there. It was the only one with a good quality pre-event.

Equipartition Theory.

Following Shapiro *et al.* (2000), the energies of compression and shear deformations are:

$$W_P = \frac{1}{2}\rho\alpha^2(\nabla\cdot\vec{u})^2 \tag{1}$$

$$W_S = \frac{1}{2}\rho\beta^2|\nabla\times\vec{u}|^2 \tag{2}$$

where α, β and ρ denote the compressional and shear wave velocities and mass density at the receiver and $\vec{u}$ is the displacement vector. Therefore, the ratio of the energy densities, W_S and W_P associated with the deformation in a solid medium at the surface is given by:

$$\frac{W_S}{W_P} = \frac{\left(\frac{\mu}{2}\right)|\nabla\times\vec{u}|^2}{\left(\frac{\lambda}{2}+\mu\right)(\nabla\cdot\vec{u})^2} \tag{3}$$

where λ and μ are the Lamé constants.

For an array of seismometers installed on the free surface of a half-space the *z*-derivatives can be obtained from the stress-free boundary condition. In fact, if stresses $\sigma_{zz}, \sigma_{zx},$ and σ_{zy} are null at *z*=0, we found that $\frac{\partial u_z}{\partial z} = \frac{2\beta^2-\alpha^2}{\alpha^2}\left(\frac{\partial u_x}{\partial x}+\frac{\partial u_y}{\partial y}\right)$, $\frac{\partial u_x}{\partial z} = -\frac{\partial u_z}{\partial x}$ and $\frac{\partial u_y}{\partial z} = -\frac{\partial u_z}{\partial y}$. Therefore, this energy ratio can be written in terms of derivatives with respect to the horizontal Cartesian coordinate system as:

$$\frac{W_S}{W_P} = \frac{1}{4}\left(\frac{\alpha}{\beta}\right)^2 \frac{4\left(\frac{\partial u_z}{\partial x}\right)^2 + 4\left(\frac{\partial u_z}{\partial y}\right)^2 + \left(\frac{\partial u_x}{\partial y} - \frac{\partial u_y}{\partial x}\right)^2}{\left(\frac{\partial u_x}{\partial x} + \frac{\partial u_y}{\partial y}\right)^2} \tag{4}$$

The energy ratio of equation 4 allowed to assess the partitioned energy in the seismic coda (Shapiro *et al.,* 2000; Hennino *et al.,* 2001; Margerin *et al*., 2009). However, we apply this ratio for the analysis of ASN records. For a diffuse field in a full-space, and considering only body waves, Weaver (1982) obtained for that ratio a value of $2(\alpha/\beta)^3$, which for a Poisson solid is 10.4. On the other hand, for ASN consisting only of surface waves, the figure is close to 6.5 (Hennino *et al.*, 2001).

Arrays at the Engineering School and the Sport Field of the UNAM and La Primavera park.

To estimate the strain energies W_S and W_P in the ASN data, two arrays of three Guralp® 6TD sensors were deployed at the yard of the Engineering School and the Sport Field (UNAM). The sensors were installed in an L-shaped array at each site with a spacing of 12 and 15 m, respectively, from the vertex station. Figure 1 shows the configuration of the arrays. The duration of the records, with common time, was approximately two hours and the absolute time was encoded in the radio signals of the GPS satellites. With this type of array, we can estimate the spatial derivatives of the displacement field in two linearly independent horizontal directions. The ASN data of the La Primavera experiment were obtained from a spatial arrangement of Guralp 6TD sensors located at La Primavera park in Zapopan, Jalisco, Mexico. The sensors were installed in an L-shaped array with a spacing of 1.5 km from the vertex station (See figure 1). During the experiment, the M_w 7.1 September 19, 2017 earthquake was recorded. The epicenter was located between Puebla and Morelos Mexican states, 12 km southeast of Axochiapan, Morelos (SSN, 2020), with an epicentral distance of approximately 500 km.

Before applying Equation 4 to the ASN data, we have preprocessed the signals removing the instrumental response and integrating the velocity records to obtain displacements. The orientation of the sensors in the array was verified at the installation time, so no rotation procedure was required. Then, we estimate the spatial derivatives of the displacements at each time sample through the following equations:

$$\frac{\partial u_i}{\partial x} = \frac{u_i^2 - u_i^1}{d}$$

$$\frac{\partial u_i}{\partial y} = \frac{u_i^3 - u_i^2}{d}; \; i = x, y, z \tag{5}$$

where u_i^n is the displacement in the i direction at station n. d is the distance between receivers.

Shapiro *et al.* (2000) indicate that the derivative estimated with finite difference differs from the exact value according to the following equation (Bodin *et al.,* 1997; Lomnitz, 1997):

$$\frac{\left[\frac{\partial u_i}{\partial x_j}\right]_{array}}{\left[\frac{\partial u_i}{\partial x_j}\right]_{exact}} = \frac{\sin(\pi L/\lambda)}{\pi L/\lambda} \tag{6}$$

where L is the distance between receivers and λ is the wavelength. If $L/\lambda \leq 0.1$ the error in the calculation of the derivatives is less than 2%.

Therefore, the available range of frequencies to estimate the derivatives of displacements, according to the interstation distances, is between 2 and 4 Hz for the Engineering School array, from 2.5 to 4.5 Hz for the Sport Field array and between 0.25 and 0.45 Hz for La Primavera array. These frequencies were obtained by applying the relationship $f = V_s/\lambda$, where f is the value of the frequency, Vs is the velocity of the S waves and λ is the wavelength. To obtain the values of Vs and λ, we use the same "L" arrangement to obtain the phase velocity of the Rayleigh waves, V_R, using SPAC (Aki, 1957). For example, assuming that the material has a Poisson coefficient of 0.25, we can estimate the velocity of the S waves form V_R as $V_s = V_R/0.92 = 600\ \frac{m}{s}$. In our case we chose the range a $0.05 \leq L/\lambda \leq 0.07$.

Chilpancingo Experiment

The ASN data used in this study were gathered at a temporary array located near Chilpancingo, Guerrero (Mexico) during June-August 1997. The array consisted of four stations installed in the corners of a square with sides of 50 m. During the experiment, 13 seismic events were well recorded.

Coda energy partition results has been reported elsewhere (Shapiro *et al.,* 2000 and Hennino *et al*., 2001). However, only event 12 has pre-event data long enough (an ASN record) to perform our analysis. We estimate the strain energies W_P and W_S for these data using the same pre-processing and methods described in Shapiro *et al.* (2000).

Experimental results

After data processing, we estimate the W_S/W_P energy ratio using equation 4. Energy equipartition among the various modes is a property of the average wavefield if the modes can be distinguished and numbered. To approximately compute the average energy ratio for each record, different moving-average windows lengths (MAWLs) are used. Margerin *et al*. (2001) and Shapiro *et al.* (2000) selected these window widths close to the "mean free-time". Nevertheless, this last parameter is complicated to estimate with traditional techniques based on attenuation studies because the effects of energy absorption and multiple scattering are related (Larose *et al.,* 2004). The mean-free-time can be related to the medium diffusivity estimated by direct measurements of energy density in terms of the diffusive acoustic model and/or the radiation transfer equations (Wegler, 2005; Wegler *et al.,* 2006). In practice, we regard the MAWL for which stabilization is reached as an estimate of the mean free-time.

Figure 2 depicts the results for the Chilpancingo array. As shown by Shapiro *et al.* (2000) and Hennino *et al.* (2001), the W_S/W_P ratio in the coda stabilizes at very different levels for the noise in the pre-event and for the direct arrivals (see figure 2-b). However, sometimes (*e.g.,* 0 to 200s) the W_S/W_P of ASN is reasonably stable with average values of 7.47 ± 0.83 while W_S/W_P of the coda is stable with average values of 7.29 ± 0.42. The fluctuations are likely due to multiple scattering of waves in the random medium and the available energy amount. Note that the W_S/W_P of ASN stabilizes for 55s MAWL while the W_S/W_P of coda only needed a 16s MAWL (reported value from Shapiro *et al.,* (2000) and Hennino *et al.,* 2001). Moreover, the W_S/W_P of ASN does not exhibit fluctuations larger than fifteen percent of the average value in the seismic coda.

For the UNAM-ES array, the W_S/W_P ratio stabilized at some time intervals with an average value of 7.28 (for example, see the interval 2,000-5,000 s), this W_S/W_P energy ratio stabilizes for a MAWL of

35 s. However, the W_S/W_P value shows fluctuations in the range from 5 to 10 for different measurements of ASN. Table 1 shows the observed and theoretical values of stabilization of the energy ratio on the free surface of a half-space with $\lambda = \mu$, as well as the experimental MAWL. The results for the Engineering School array are displayed in figure 3.

For the UNAM-SF array, the W_S/W_P energy ratio stabilizes at an average of 2.9 ± 0.47 with a MAWL of 45 s. This average is very far from the expected theoretical value of 7.19 for equipartitioned elastic waves at the surface of a homogeneous Poissonian half-space. In fact, Margerin *et al*., (2009) found similar energy values, W_S/W_P =2.8, for 10 earthquakes recorded on a dense array located at Pinyon Flats Observatory, California. In order to explain these values, they developed a theory of equipartition in a layered elastic-space using a rigorous spectral decomposition of the elastic wave equation. They observed that, close to the resonance frequency, a decrease of the W_S/W_P takes place.

The site La Primavera is within the Mexican Transverse Neo Volcanic Belt and it is characterized by intercalations of lava and pyroclastic materials of andesitic-basaltic composition. For volcanic environments, the energy equipartition can hardly be reached since they generally consist of weakly diffusive and strongly scattering material (Wegler 2003, De Siena *et al.* 2013, 2016). In principle, the results will strongly depend on scale, topography and boundary conditions. The experiment at La Primavera site is described in figure 4. We find that, after the seismic event (0.3 to 0.5 hrs.), the W_S/W_P is unstable and well below the expected theoretical value of equipartition (< 6.5). However, as time progresses, the W_S/W_P oscillates between 6 and 10. These values are within the ratio expected for a purely Rayleigh wave field and a purely body-wave field ratio. Finally, it tends to stabilize at 7.1 ± 0.5 (see, for example, the interval from 1.5 to 3 hrs. in figure 3c). This stabilization occurs for a MAWL of 150s. The partitioning regime is reached for long windows. It indicates that the typical dimension of heterogeneity's typical dimension is about the size of the wavelength (Shapiro *et al.* 2000).

In order to explore some consequences of the stabilization of the W_S/W_P energy ratio, we calculated the horizontal-to-vertical spectral ratio (HVSR) for the dataset of the Primavera experiment. A 150s window length was used (the estimated MAWL) with 99% overlap was used to obtain the HVSR, as well as a 5% cosine taper and a logarithmic-window smoothing of 35% relative bandwidth (Konno and Ohmachi, 1998) were used. The HVSR in a frequency range between 0.2-20 Hz is shown in figure 4 d-f as a function of time, together with their corresponding average HVSR curves. From these results, we observe that during the seismic pre-event, the HVSR is stable in their shape and amplitude (0-0.1 hrs.). However, when the seismic event begins, the HVSR becomes unstable and does not reach the average amplitude during the first arrivals. After the first arrivals, there is a time interval (surface waves arrivals) where the amplitude stabilizes. On the other hand, in the time interval 0.2 - 0.4 hrs. we find that the HVSR is unstable and its shape differs from that found in windows dominated by ASN. While both the seismic coda and the ASN are present, the HVSR gradually converges in shape and amplitude towards the level found in the pre-event (ASN). For a distant earthquake like this, frequencies higher than, say 0.5 Hz, are almost cancelled by anelastic absorption, and the remaining energy is likely to be channeled by crustal structures making guided quasi-ballistic waves with scarce scattering. Therefore, at these frequencies the equilibration due to scattering takes more time than for receivers at close-range. Certainly, the subject requires attention but now it is beyond the focus of this research. These long period fluctuations may imply large scale structures. Careful analysis is required to understand their origin. An extreme case is the breakdown of equipartition for large period (10 to 40 s) coda waves (Sens-Schönfelder, *et al.* 2015). Based on these results, we observe a relationship between the stabilizations of the W_S/W_P energy ratio and the HVSR. If the W_S/W_P does not stabilize to the expected theoretical values (between values of 6 and 10) then, the HVSR does not recover its average amplitude and shape. This behavior is observed in figure 4 for the time interval between 0.2 to 0.4 hrs. On the other hand, the oscillations in the W_S/W_P are reflected in the amplitude of the HVSR, that is, while the W_S/W_P exceeds the average value, the amplitude of the HVSR increases and it decreases when WS/WP is low. An example of this is observed for the time intervals of 0.7 – 0.9 hr. and 0.9 - 1.1 hrs. (figure 4). This confirms that, in absence of energy equipartition in ASN or earthquake data, the shape and amplitude of the HVSR are disturbed and, consequently, Green's functions cannot be recovered.

The conspicuous fluctuations of the W_S/W_P energy ratio in some time windows reflect the variability of different mode contents in the wavefield. The energy stabilization of the seismic coda represents a genuine process of multiple scattering and diffraction (Hennino *et al*., 2001). Moreover, the ASN can be interpreted, based on the clear stabilization of the W_S/W_P, as a diffusive regime as well. Summing up the observations, we find that W_S/W_P for ASN is stable. The equilibration between the different modes of vibration occurs faster in the seismic coda compared to the ASN. The W_S/W_P stabilization within the ASN is a process which anticipates the diffusion regime. Moreover, Margerin *et al.* (2000) pointed out that the time evolution of the W_S/W_P could be used as a marker for the different scattering mechanisms. Finally, to observe the effect of MAWL on the W_S/W_P energy ratio, different MAWLs were applied. Figure 5 shows the stabilization of the W_S/W_P for the arrays as the MAWL increases.

Discussion and conclusions

Using the W_S/W_P energy ratio, applied the procedure described by Shapiro *et al.* (2000) to separate the energies and follow their time evolution, we studied the stabilization of energies carried by ambient seismic noise (ASN) in different settings:

(1) The Chilpancingo (Guerrero, Mexico) Array at a relatively firm site using the ASN in the pre-event of an earthquake that allowed the first experimental evidence of equipartition in the coda (Shapiro *et al.,* 2000 and Hennino *et al*., 2001).

(2) The UNAM's Engineering School experiment for ASN. The site is a weathered basalt in the yard of the school building.

(3) The UNAM's Sport field experiment for ASN. The site is characterized by a very soft soil layer on weathered basalt at some meters deep.

(4) The La Primavera experiment to analyze ASN in the post-event. This site is within the Mexican Transverse Neo Volcanic Belt, which is characterized by intercalations of lava and pyroclastic materials of andesitic-basaltic composition.

UNAM's Engineering School and La Primavera experiments we observed that the ratio remains stable for a long time with ±15% relative error with respect to the theoretical value of 7.19 for equipartitioned elastic waves at the surface. However, it occasionally exhibits fluctuations between the expected theoretical values for body waves W_S/W_P=9.76 and for Rayleigh waves W_S/W_P=6.46 (implying deviations of +35% and -10% form 7.19, respectively, figure 6). Based on the results at La

Primavera, we observe a relationship between the stabilizations of the W_S/W_P energy ratio and the HVSR. If the W_S/W_P does not stabilize to the expected theoretical values (between values of 6 and 10) then, the HVSR does not recover its average amplitude and shape. The results from the UNAM's Sports field show that the W_S/W_P stabilizes at around 2.9 ± 0.47, very far from the expected theoretical value of 7.19 for equipartitioned elastic waves at the surface of a homogeneous Poissonian half-space. Even though this result deserves further scrutiny, the soft and thin sediments of that site likely played role in that low average (Poppeliers 2015, Margerin *et al.* 2009). Poppeliers (2015) observed that the near-surface geologic structure influences the W_S/W_P energy ratio. Margerin *et al.* (2009) modeled this effect for an arbitrary layered elastic media using the spectral decomposition of the elastodynamic operator.

We find that, for the Chilpancingo array, the W_S/W_P energy ratio in the pre-event of an earthquake stabilizes for windows longer than those needed for seismic coda. Moreover, whereas the W_S/W_P is 7.29 ± 0.42 for the seismic coda, this ratio stabilizes at 7.47 ± 0.83 in the pre-event. In addition, the energy partition in the coda is reached quickly, after a few seconds of MAWL. Figure 6 shows the stabilization of the W_S/W_P for the arrays. The interval of ±15% relative error with respect to the theoretical value for equipartitioned elastic waves at the surface (7.19) is shown with a gray band. The stabilization of the W_S/W_P energy ratio in the ASN is a process that anticipates that the wave field reaches a diffusion regime. This exploration into the noise in various settings strongly supports the idea that ambient seismic noise, like the coda, is a genuine multiple scattering process. Therefore, the corresponding processing must be the same to exploit its diffuse field nature and justifies the use of HVSR in the theoretical context of diffusion. In contrast to Mulargia (2012) remark that ASN is not diffuse, we show that approximate equipartition, implicit in the S and P energy ratio (W_S/W_P), clearly emerges and suggests that the ASN could be diffuse. Recently, a time windowing scheme has been proposed to enhance diffuse properties of the field (Weaver and Yoritomo, 2018). Therefore, the corresponding processing must be the same for ASN and coda to exploit the diffuse field nature and the results justify the use of HVSR in the theoretical context of diffusion.

Data and Resources

The Chilpancingo data that support the findings of this study are available on request from the author

Campillo, M. (michel.campillo@univ-grenoble-alpes.fr). The datasets for Engineering School, Sports Field and La Primavera are available on request from the corresponding author Piña-Flores, J. (jpf@unam.mx). The seismic data were preprocessed with MATLAB® Version: 9.8.0.1359463 (R2020a) Update 1 (License Number 40816183).

Acknowledgements

Thanks are given to Dr. Adrien Oth, Dr. Thomas L. Pratt and three anonymous reviewers for their constructive remarks. The authors also thank L. Margerin and N. M. Shapiro for providing them with the Chilpancingo array data and their keen, constructive and insightful remarks, to J. F. Lermo-Samaniego and his working group for providing the seismic data of the La Primavera park, and to J. E. Plata and M. G. Sánchez of Universidad Nacional Autónoma de México (UNAM) for locating useful references. This work has been partially supported by the Mexican National Council of Science and Technology (CONACYT) through the National Scholarship CONACYT number 449268, by UNAM–Dirección General Asuntos del Personal Académico (DGAPA) projects PAPIIT IN117119, IN107720 and PAPIME PE105520, and by Ministerio de Economía y Competitividad de España and European Regional Development Fund (ERDF) under Project CGL2014-59908/JIN. M. C. acknowledges the support from the European Research Council (ERC) under the European Union Horizon 2020 research and innovation program (Grant Agreement Number 742335, F-IMAGE project).

References

Aki, K. (1957). Space and time spectra of stationary stochastic waves, with special reference to microtremores, *Bull. Earth. Res. Inst.,* **35,** 415-456.

Aki, K. and Chouet, B. (1975). Origin of coda waves: source, attenuation, and scattering effects, *J. Geophys. Res.,* **80**(23), 3322-3342.

Ardhuin, F., Stutzmann, E., Schimmel, M. and Mangeney, A. (2011). Ocean wave sources of seismic noise, *J. Geophys. Res.- Oceans*, **116**, C09004.

Asten, M.W. and Henstridge, J.D. (1984). Arrays estimators and the use of microseisms for reconnaissance of sedimentary basins, *Geophysics* **49**(11), 1828-1837.

Bodin, P., Gomberg J., Singh S. K. and Santoyo, M. (1997). Dynamic deformations of shallow sediments in the Valley of Mexico, Part I: three dimensional strains and rotations recorded on a seismic array, *Bull. Seismol. Soc. Am.*, **87,** 528-539.

Campillo, M. (2006). Phase and Correlation in 'Random' Seismic Fields and the Reconstruction of the Green Function, *Pure Appl. Geophys.,* **163** (2-3), 475-502.

De Siena, L., Del Pezzo, E., Thomas, C., Curtis, A. and Margerin, L. (2013). Seismic energy envelopes in volcanic media: in need of boundary conditions. *Geophys. J. Int.* **195**, 1102-1119.

De Siena, L., Calvet, C., Watson, K.J., Jonkers, A.R.T. and Thomas, C. (2016). Seismic scattering and absorption mapping of debris flows, feeding paths, and tectonic units at Mount St. Helens volcano. *Earth Planet. Sci. Lett*. **442**, 21-31.

Friederich, A., Kruger F. and Klinge, K. (1998). Ocean-generated microseismic noise located with the GRFO array, *J. Seismol.* **2**, 47-64.

García-Jerez, A., Piña-Flores, J., Sánchez-Sesma, F. J., Luzón, F. and Perton, M. (2016). A computer code for forward calculation and inversion of the H/V spectral ratio under the diffuse field assumption, *Comput. Geosci*. **97**, 67-78.

Garcia-Jerez, A., Seivane, H., Navarro, M., Martínez-Segura, M. and Piña-Flores, J. (2019). Joint analysis of Rayleigh-wave dispersion curves and diffuse-field HVSR for site characterization: The case of El Ejido town (SE Spain). *Soil Dynam. Earthquake Eng.* **121.** 102-120.

Gudmundsson, O., Khan, A. and Voss, P. (2007). Rayleigh-wave group-velocity of the Icelandic crust from correlation of ambient seismic noise, *Geophys. Res. Lett.,* **34**(14), L14314.

Hennino, R., Tregoures, N., Shapiro, N.M., Margerin, L., Campillo, M., Van Tiggelen B.A. and Weaver, R. L. (2001). Observation of equipartition of seismic waves, *Phys. Rev. Lett.,* **86**, 3447-3450.

Kanai, K., Tanaka, T. and Okada, K. (1954). Measurement of the microtremor, *Bull. Earthquake Res. Inst.* Tokio Univ. **32,** 199-210.

Konno, K. and Ohmachi, T. (1998). Ground-motion characteristics estimated from spectral ratio between horizontal and vertical components of microtremor. *Bull. Seismol. Soc. Am.* **88** (1), 228-241.

Larose, E., Margerin, L., Campillo, M. and Van Tiggelen, B.A. (2004). Weak localization of seismic waves, *Phys. Rev. Lett*., **93**, 048501.

Liu, X. and Ben-Zion, Y. (2016). Estimating correlations of neighbouring frequencies in ambient seismic noise, *Geophys. J. Intl*. **206**, 1065-1075.

Lomnitz, C. (1997). Frequency response of a strainmeter, *Bull. Seismol. Soc. Am.*, **87,** 1078-1080.

Margerin, L., Campillo, M. and Van Tiggelen, B. (2000). Monte Carlo simulation of multiple scattering of elastic waves. *J. Geophys. Res.: Solid Earth* **105**.B4 7873-7892.

Margerin, L., Van Tiggelen, B. A. and Campillo, M. (2001). Effect of absorption on energy partition of elastic waves in the seismic coda, *Bull. Seismol. Soc. Am.*, **91**(3), 624-627.

Margerin, L., Campillo, M., Van Tiggelen, B. A. and Hennino, R. (2009). Energy partition of seismic coda waves in layered media: Theory and application to Pinyon Flats Observatory, *Geophys. J. Int.* **177**(2), 571-585.

Matsushima, S., Kosaka, H. and Kawase, H. (2017). Directionally dependent horizontal-to-vertical spectral ratios of microtremors at Onahama, Fukushima, Japan, *Earth, Planets. Space*. **69**(1), 96.

Mulargia, F. (2012). The seismic noise wavefield is not diffuse. *J. Acoust. Soc. Am*., **131**, 2853-2858.

Nakamura, Y. (1989). A method for dynamic characteristics estimation of subsurface using microtremor on ground surface, *QR of RTRI* **30**(1), 25-33.

Nakamura, Y. (2000), Clear identification of fundamental idea of Nakamura's technique and its applications, 'Proceedings of the 12th World Conference on Earthquake Engineering', Auckland New

Zealand.

Papanicolaou, G. C., Ryzhik, L. V. and Keller. J. B. (1996). Stability of the P- to S-energy ratio in the diffusive regime. *Bull. Seismol. Soc. Am.*, **86,** 1107-1115.

Pérez-Ruiz, J. A., Luzón, F. and Sánchez-Sesma, F. J. (2008). Retrieval of elastic Green’s tensor near a cylindrical inhomogeneity from vector correlations, *Commun. Comput. Phys.*, **3**(1), 250-270.

Perton, M. and Sánchez-Sesma, F. J. (2016). Green's function calculation from equipartition theorem, *J. Acoust. Soc. Am*., **140**(2), 1309-1318.

Perton, M., Spica, Z. and Caudron, C. (2018). Inversion of the horizontal-to-vertical spectral ratio in presence of strong lateral heterogeneity, *Geophys. J. Int.*, **212**, 930-941.

Piña-Flores, J., Perton, M., García-Jerez, A., Carmona, E., Luzón, F., Molina-Villegas, J. C. and Sánchez-Sesma, F. J. (2017). The inversion of spectral ratio H/V in a layered system using the Diffuse Field Assumption (DFA), *Geophys. J. Int.*, **208**(1), 577-588.

Piña-Flores, J., Cárdenas-Soto, M., Sarabia-González, A., García-Jerez, A., Sierra-Álvarez, C. A., Sáenz-Castillo, M. A., Luzón, F. and Sánchez-Sesma, F. J. (2021). Imaging the structure of the Sun Pyramid (Teotihuacán, Mexico) from passive seismic methods. *Eng. Geol.*, **281,** 105969.

Poppeliers, C. (2015). The Effects of the Near-Surface Geology on P-S Strain Energy Partitioning of Diffusive Seismic Coda: Preliminary Observations and Results. *Bull. Seismol. Soc. Am.*, **105, 4.** 2143-2150,

Przybilla, J., Korn, M. and Wegler, U. (2006). Radiative transfer of elastic waves versus finite difference simulations in two-dimensional random media, *J. Geophys. Res.*, **111**, B04305.

Rhie, J. and Romanowicz, B., (2004). Excitation of Earth's continuous free oscillations by atmosphere-ocean-seafloor coupling. *Nature*, **431**(7008), 552-556. doi: 10.1038/nature02942

Ritzwoller, M. H., Lin, F. C. and Shen, W. (2011). Ambient noise tomography with a large seismic array, *Comp. Rendus. Geosci.*, **343**(8), 558-570.

Sabra, K.G., Gerstoft, P., Roux, P., Kuperman, W.A. and Fehler, M.C. (2005). Extracting timedomain Green's function estimates from ambient seismic noise, *Geophys. Res. Lett.,* **32**, L03310,

Sánchez-Sesma, F. J., Pérez-Ruiz, J. A., Campillo, M. and Luzón, F. (2006). Elastodynamic 2D Green function retrieval from cross-correlation: Canonical inclusion problem', *Geophys. Res. Lett.,* **33**, L13305.

Sánchez-Sesma, F. J., Rodríguez, M., Iturrarán-Viveros, U., Luzón, F., Campillo, M., Margerin, L., García-Jerez, A., Suárez, M., Santoyo, M. A. and Rodríguez-Castellanos, A. (2011a). A theory for microtremor H/V spectral ratio: application for a layered medium, *Geophys. J. Int*., **186**, 221-225.

Sánchez-Sesma, F. J., Weaver, R. L., Kawase, H., Matsushima, S., Luzón, F. and Campillo, M. (2011b). Energy partitions among elastic waves for dynamic surface loads in a semi-infinite solid, *Bull. Seismol. Soc. Am.*, **101**(4), 1704-1709.

Saygin, E. and Kennett, B. L. (2010). Ambient seismic noise tomography of Australian continent. *Tectonophysics*, **481**(1), 116-125.

Sens-Schönfelder, C., Snieder, R. and Stähler, S. C. (2015). The lack of equipartitioning in global body wave coda, *Geophys. Res. Lett*. 42, 7483- 7489.

Shapiro, N.M., Campillo, M., Margerin, L., Singh, S.K., Kostoglodov, V. and Pacheco, J. (2000). The energy partitioning and the diffusive character of the seismic coda. *Bull. Seismol. Soc. Am.*, **90**, 655-665.

Shapiro, N.M. and Campillo, M. (2004). Emergence of broadband Rayleigh waves from correlations of the ambient seismic noise, *Geophys. Res. Lett.,* **31**, L07614.

Shapiro, N.M., Campillo, M., Stehly, L. and Ritzwoller, M. (2005). High resolution surface wave tomography from ambient seismic noise, *Science.,* **307**, 1615-1618.

Spica, Z., Caudron, C., Perton, M., Lecocq, T., Camelbeeck, T., Legrand, D., Piña-Flores, J., Iglesias, A. and Syahbana, D. K. (2015). Velocity models and site effects at Kawah Ijen volcano and Ijen caldera (Indonesia) determined from ambient noise cross-correlations and directional energy density spectral ratios, *J. Volcanol. Geoth. Res*., **302**, 173-189.

SSN (2020): Universidad Nacional Autónoma de México, Instituto de Geofísica, Servicio Sismológico Nacional, México. Dirección electrónica: http://www.ssn.unam.mx

Ward, K. M., Porter, R. C., Zandt, G., Beck, S. L., Wagner, L. S., Minaya, E. and Tavera, H., (2013). Ambient noise tomography across the Central Andes, *Geophys. J. Int.*, **196** (2), 1264-1265.

Weaver, R. L. (1982). On diffuse waves in solid media, *J. Acoust. Soc. Am*., **71**(6), 1608-1609.

Weaver, R. L. (1985). Diffuse elastic waves at a free surface, *J. Acoust. Soc. Am*., **78**(1), 131-136.

Weaver, R., Froment, B. and Campillo, M. (2009). On the correlation of non-isotropically distributed ballistic scalar diffuse waves. *J. Acoust. Soc. Am*, **126**(4), 1817-1826.

Weaver, R. L. and Yoritomo, J.Y. (2018). Temporally weighting a time varying noise field to improve Green function retrieval. *J. Acoust. Soc. Am*. **143**(6), 3706-3719.

Wegler, U. (2005). Diffusion of seismic waves in layered media: boundary conditions and analytical solutions, *Geophys. J. Int.* **163**, 1123-1135.

Wegler, U., Korn, M. and Przybilla, J. (2006). Modeling full seismogram envelopes using radiative transfer theory with born scattering coefficients, *Pure Appl. Geophys*., **163,** 503-531.

Wegler, U. (2003). Analysis of multiple scattering at Vesuvius volcano, Italy, using data of the TomoVes active seismic experiment. *J. Volcanol. Geoth. Res.* **128**. 45-63.

Yang, Y., M. H. Ritzwoller, A. L. Levshin, and N. M. Shapiro (2007). Ambient noise Rayleigh wave tomography across Europe, Geophys. J. Int. 168, 259–274.

Zheng, S., Sun, X., Song, X., Yang, Y. and Ritzwoller, M. H. (2008). Surface wave tomography of

China from ambient seismic noise correlation, *Geochem. Geophys. Geosyst.,* **9** (5).

Figures

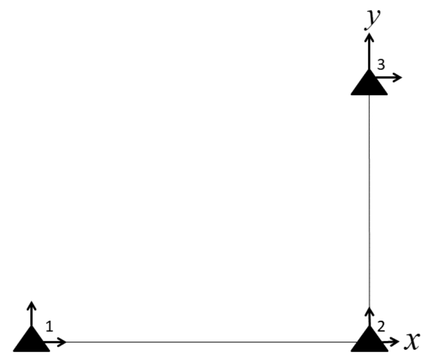

Figure 1.- L-shape array configuration used in the Engineering School, the Sports Field (UNAM) and La Primavera park. The arrows on the triangles indicate the orientation of each sensor.

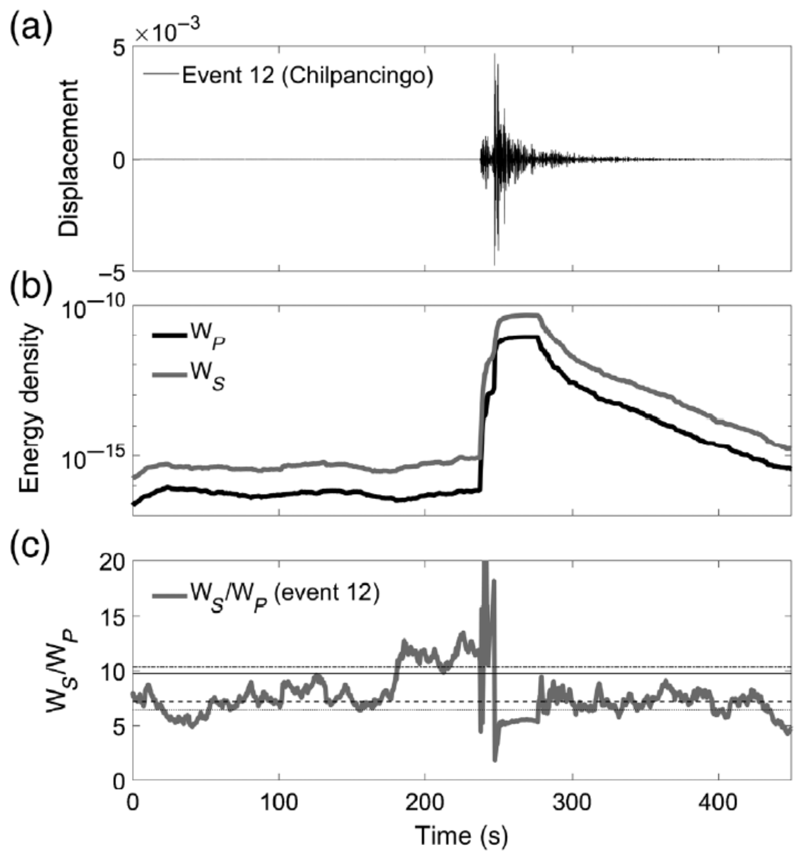

Figure 2.- Measurements of the W_P and W_S energies and their W_S/W_P energy ratio for the 1999 Chilpancingo array. (a) The record of the vertical component filtered between 1 and 3 Hz. (b) The W_P and W_S energies depicted correspond to a moving average windows length (MAWL) of 16 s for coda (Shapiro *et al.,* 2000; Hennino *et al.,* 2001) and of 55s for the pre-event noise. The energy densities of coda range from four to five orders of magnitude above the of pre-event (noise) levels. (c) The W_S/W_P energy ratio for data. The horizontal lines represent, from the lowest to the highest, the theoretical value of WS/WP for bulk waves only at z = 0; the theoretical value of WS/WP at z = 0 (for a Poisson solid and all the wave modes); the theoretical value of WS/WP for Rayleigh waves only at z = 0; and the theoretical value of W_S/W_P at $z = \infty$. These variations are well within expected variations due to transients but, giving the huge difference in energy levels, the stability of ratios is remarkable.

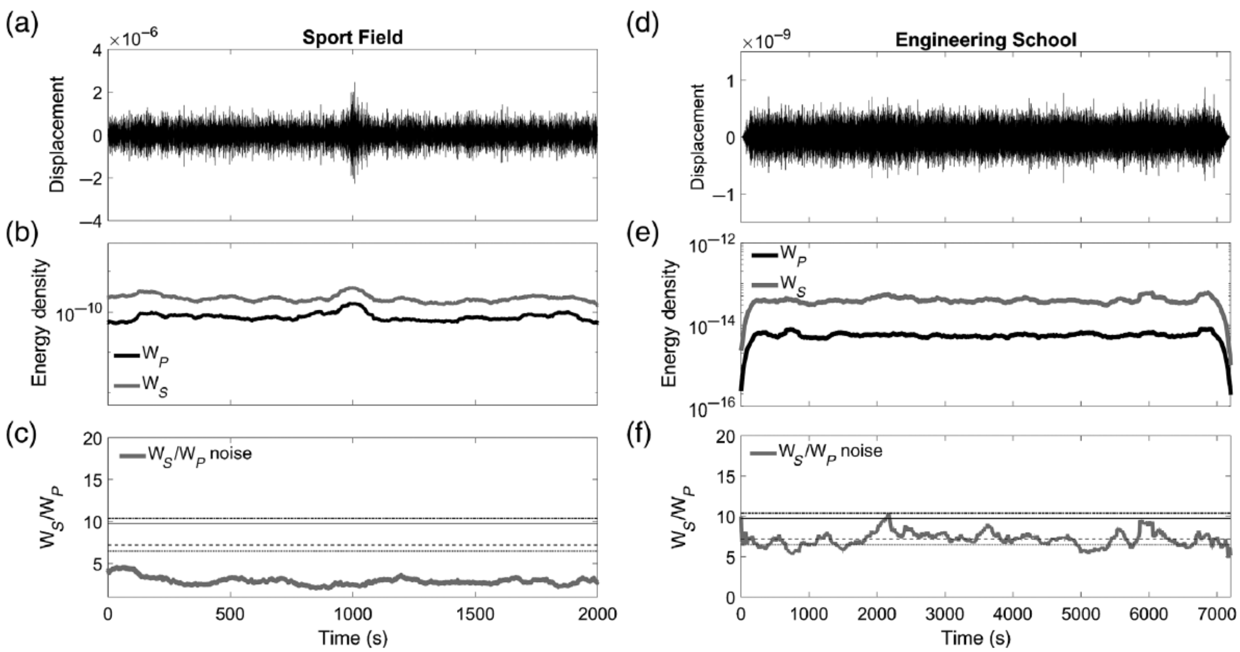

Figure 3.- Measurements of the W_P and W_S energies and their ratio W_S/W_P at both the Engineering School and the Sports field (UNAM's main campus). (a) The vertical component, filtered between 2 and 4 Hz, recorded at the Sport field. (b) The W_P and W_S energies with a 32s MAWL. (c) The W_S/W_P. (d) The vertical component, filtered between 2.5 and 4.5 Hz, recorded at the Engineering School. (e) The W_P and W_S energies are shown with a 45s MAWL. (f) The W_S/W_P ratio for ASN data. The horizontal lines represent, from the lowest to the highest, the theoretical value of WS/WP for bulk waves only at z = 0; the theoretical value of WS/WP at z = 0 (for a Poisson solid and all the wave modes); the theoretical value of WS/WP for Rayleigh waves only at z = 0; and the theoretical value of W_S/W_P at $z = \infty$.

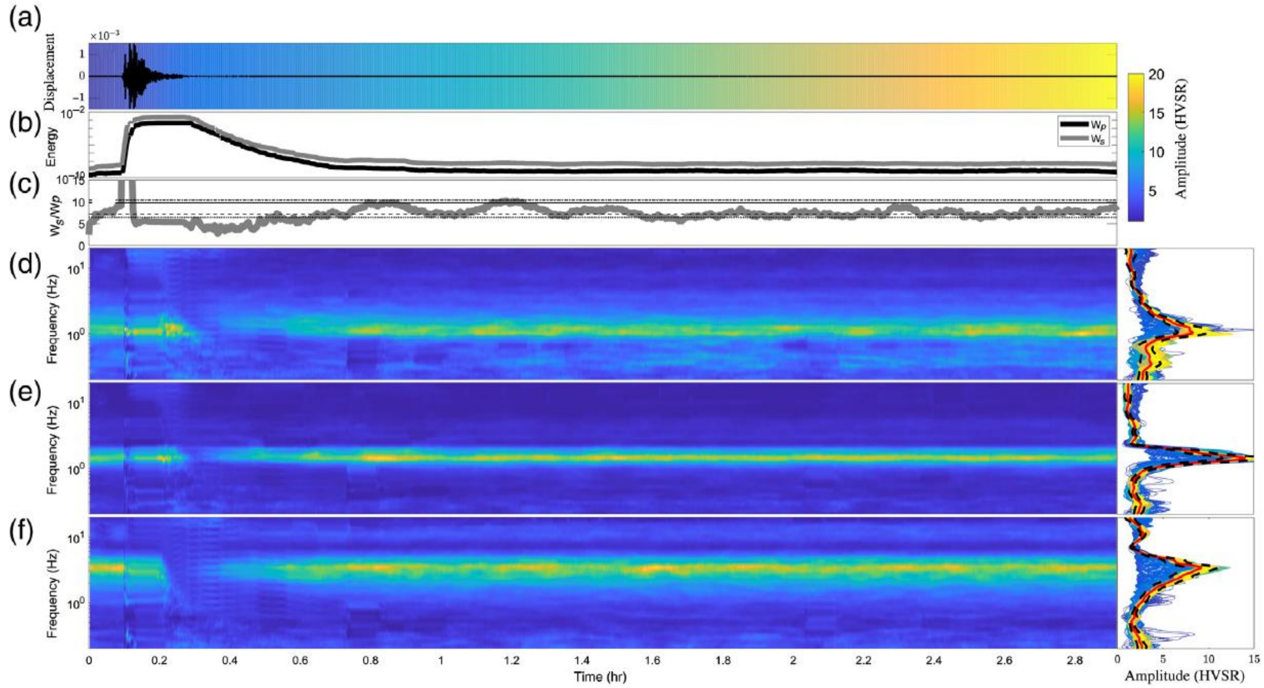

Figure 4.- Measurements of the W_P and W_S energies and their ratio W_S/W_P at the La Primavera (Zapopan, Jalisco) array. Panel a) shows the vertical component, filtered between 0.2 and 0.4 Hz. The vertical striations represent the beginning of the time windows analyzed. Panel b) depicts the W_P and W_S energies for a 150s MAWL and panel c) displays the W_S/W_P ratio. The horizontal lines represent, from the lowest to the highest, the theoretical value of WS/WP for bulk waves only at z = 0; the theoretical value of WS/WP at z = 0 for all the wave modes; the theoretical value of WS/WP for Rayleigh waves only at z = 0; and the theoretical value of W_S/W_P at $z = \infty$. These calculations correspond to a Poisson solid. Panels d), e) and f) show, for each station of the array, the evolution of the horizontal-to-vertical spectral ratio (HVSR) as a function of time. The colorbar represents the HVRS amplitude in panels d), e) and f). Note that the HVSR for each station reflects a significant site effect.

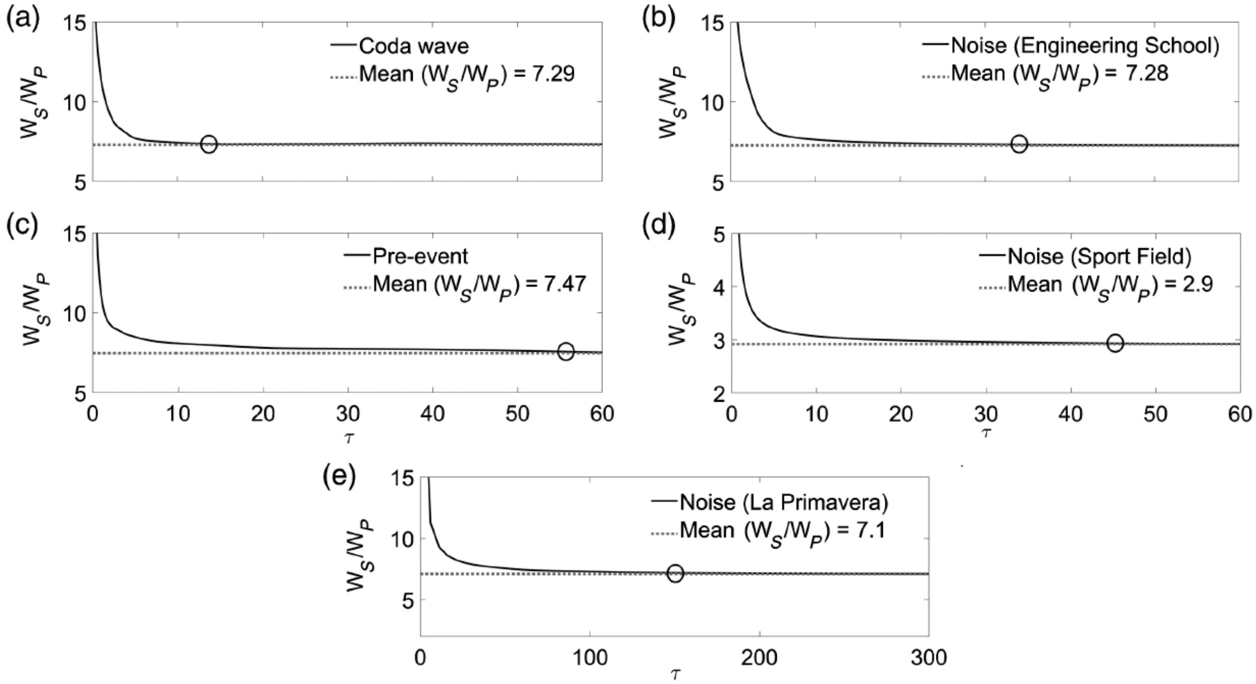

Figure 5.-Measurements of W_S/W_P versus the MAWL (τ) for the analyzed experiments. Solid lines represent the average W_S/W_P. The dotted lines represent the stabilization values of the averaged W_S/W_P. The open circles mark the MAWL from which the W_S/W_P stabilizes (i.e., our estimate of the mean free time). a) The W_S/W_P for coda wave for the Chilpancingo experiments, requiring 16 s MAWL (reported value by Shapiro *et al*., (2000) and Hennino *et al.,* 2001). b) W_S/W_P in the pre-event of the same record needed 55 s. c) The stabilization of W_S/W_P for ASN at the Engineering School (MAWL of ~32s). d) The stabilization of W_S/W_P for ASN at UNAM-SF (MAWL of ~45s). e) Results for ASN at La Primavera park, where 150 s of MAWL were required to reach equipartition.

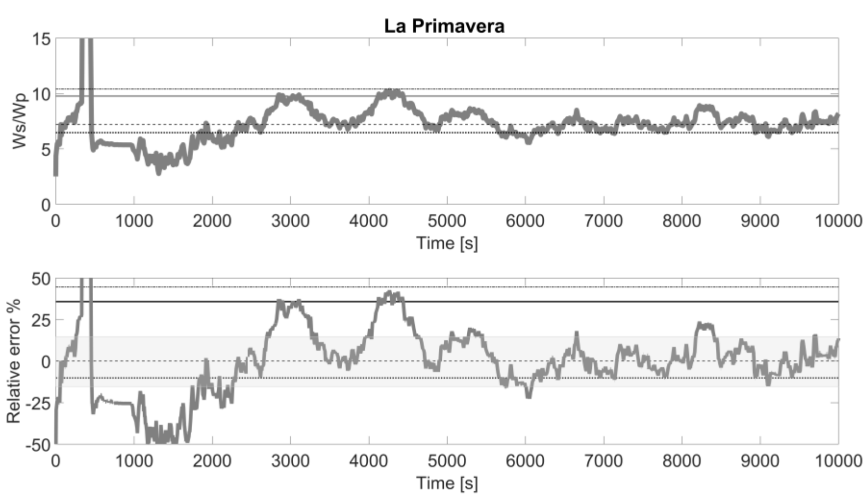

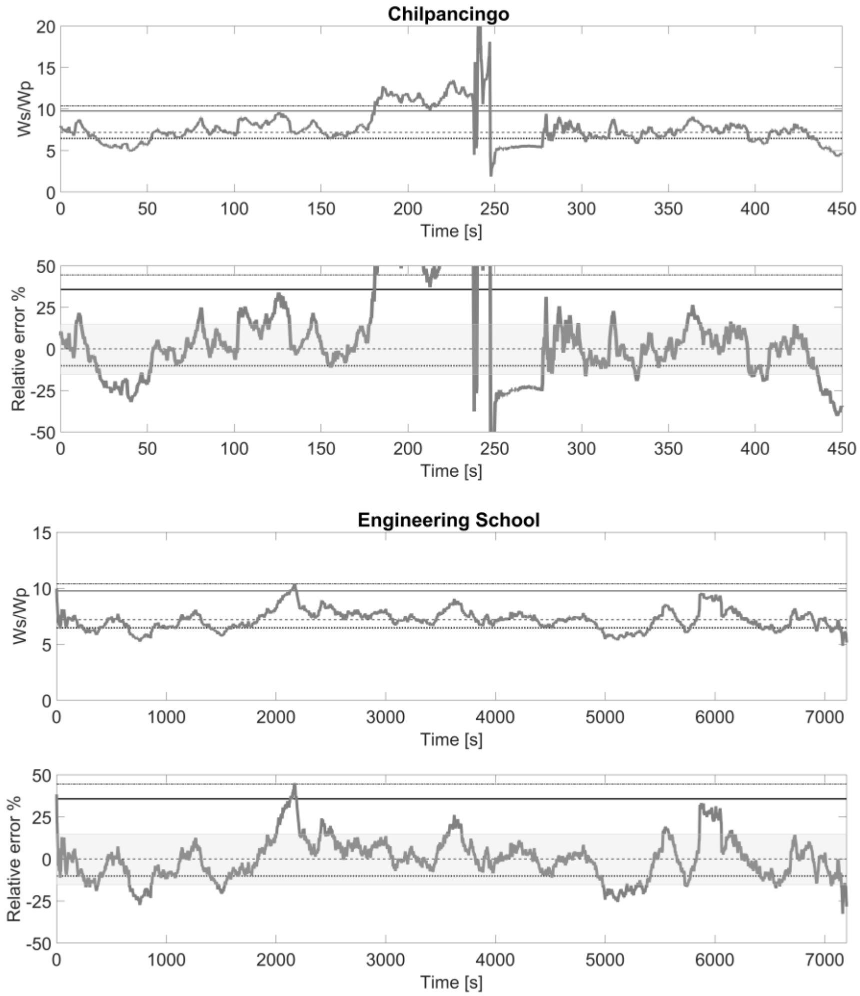

Figure 6.- Measurements of the ratio W_S/W_P at the Chilpancingo and Engineering School and the Sports field (UNAM's main campus). Upper panels display the W_S/W_P values (gray line), and bottom panels display the relative error of W_S/W_P values (gray line). The horizontal lines represent, from the lowest to the highest, the theoretical value of W_S/W_P for bulk waves only at $z = 0$; the theoretical value of W_S/W_P at $z = 0$ (for a Poisson solid and all the wave modes); the theoretical value of W_S/W_P for Rayleigh waves only at $z = 0$; and the theoretical value of W_S/W_P at $z=\infty$. The gray bands represent ±15% relative error with respect to the theoretical value of 7.19 for equipartitioned elastic waves at the surface.

Table 1 Comparison between P-wave and S-wave energies (W_S/W_P) of the data and theoretical values on free surface (z=0). Theoretical values are obtained from Hennino *et al.,* (2001).

Dataset	**Data z=0**	**Theory z=0**	**Theory z=∞**	**Theory Rayleigh only z=0**	**Theory Bulk only z=0**	***MAWL (s)**
Seismic Coda	7.29±0.42	7.19	10.39	6.46	9.76	16
Pre event Noise	7.47±0.83	7.19	10.39	6.46	9.76	55
Engineering School	7.28±0.88	7.19	10.39	6.46	9.76	32
Sport Field	2.9±0.47	7.19	10.39	6.46	9.76	45
La Primavera	7.1±0.5	7.19	10.39	6.46	9.76	150

*MAWL is moving-average windows length to compute the average energy ratio for each record.